Conditions Necessary for Capillary Hysteresis in Porous Media: Tests of Grain-size and Surface Tension Influences

Tetsu K. Tokunaga, Keith R. Olson, and Jiamin Wan
Earth Sciences Division, E.O. Lawrence Berkeley National Laboratory Berkeley, California

Abstract

Hysteresis in the relation between water saturation and matric potential is generally regarded as a basic aspect of unsaturated porous media. However, the nature of an upper length scale limit for saturation hysteresis has not been previously addressed. Since hysteresis depends on whether or not capillary rise occurs at the grain-scale, this criterion was used to predict required combinations of grain-size, surface tension, fluid-fluid density differences, and acceleration in monodisperse systems. The Haines number (Ha), comprised of the aforementioned variables, is proposed as a dimensionless number useful for separating hysteretic (Ha < 15) versus nonhysteretic (Ha > 15) behavior. Vanishing of hysteresis was predicted to occur for grain-sizes greater than 10.4 ±0.5 mm, for water-air systems under the acceleration of ordinary gravity, based on Miller-Miller scaling and Haines' original model for hysteresis. Disappearance of hysteresis was tested through measurements of drainage and wetting curves of sands and gravels, and occurs between grain-sizes of 10 and 14 mm (standard conditions). The influence of surface tension was tested through measurements of moisture retention in 7 mm gravel, without and with a surfactant (sodium dodecylbenzenesulfonate, SDBS). The ordinary water system (Ha = 7) exhibited hysteresis, while the SDBS system (Ha = 18) did not. The experiments completed in this study indicate that hysteresis in moisture retention relations has an upper limit at Ha = 16 ±2, and show that hysteresis is not a fundamental feature of unsaturated porous media.

1. Introduction

The degree of water saturation (S) strongly influences water flow, transport of solutes and heat, and mechanical properties of porous media. The monotonic decrease of the matric potential (ψ) with decreased saturation reflects the combination of capillary and adsorptive influences in lowering the free energy of soil water. In the early decades of soil physics, it was assumed that the $S(\psi)$ relation in a given system represented a series of unique equilibrium conditions [e.g., Buckingham, 1907; Fisher, 1928; Richards, 1928]. Since the classic work of W. B. Haines [1930], hysteresis in the $S(\psi)$ relation has become regarded as a basic aspect of soil water behavior, and his pore-scale model is now used in other fields, most notably petroleum engineering and material sciences [e.g., Dullien, 1992; Gregg and Sing, 1982]. In the latter context, Haines' ink-bottle model has been applied to condensation in nanometer scale pores [Gregg and Sing, 1982; Ravikovitch and Neimark, 2002; Morishige and Tateishi, 2003]. At any given potential, the equilibrium saturation level obtained by draining a system is greater than or equal to that obtained by wetting a system to the same potential (Figure 1a). While hysteresis in moisture characteristic relations has several causes, Haines showed that it fundamentally arises because of the existence of different pore-sizes within granular media, and because of the inverse relation between capillary pressure and pore-size. Over the past 70 years, innumerable accounts of hysteresis in moisture retention relations have been reported. Although the nanoscale limit to condensate hysteresis has been identified [Ravikovitch and Neimark, 2002], the larger scale limit relevant in hydrology has not. In this study, we consider conditions that lead to the disappearance of capillary hysteresis in porous media, with particular attention given to identifying an upper grain-size limit for saturation hysteresis. Since hysteresis depends on the competing influences of

capillary (surface) and gravity (body) forces, it will be shown that the general conditions necessary for capillary hysteresis are predictable from the scale dependence of these forces. The predictions were tested through measurements of drainage and wetting curves of sands and gravels. Although this study focuses on water and air as the fluid phases occupying pores, the general results are expected to apply to other combinations of fluids such as oil-gas and oil-water.

2. Predicting Limits of Capillary Hysteresis

2.1. Pore-scale prediction

In capillary models of variably saturated porous media, the basic cause of $S(\psi)$ hysteresis arises from the pore-size distribution. The combination of the Young-Laplace relation and Pascal's law leads to the equation for the dependence of equilibrium capillary rise height on effective pore-radius (R), the fluid-fluid surface tension (σ), the liquid's density (ρ), and gravity (g)

$$h = -\frac{\psi}{\rho g} = \frac{2\sigma}{\rho g R} \tag{1}$$

assuming a contact angle of zero. More generally, the acceleration (ordinarily due to gravity), wettability, and densities of the 2 immiscible fluid phases influence h. Here, we focus attention on water and air in pore spaces, and main drainage and wetting curves (rather than intermediate scanning curves). Because of the above capillary relation, systems containing a distribution of pore-sizes equilibrate to different levels of water saturation depending on wetting history. Higher S values are maintained at any given ψ during desaturation, relative to rewetting, since drainage is controlled by narrow pore throats that require lower energy to empty. Conversely, rewetting requires increasing the potential high enough (closer to zero) to allow water entry into large pore bodies. Other factors contributing to hysteresis include phase entrapment resulting from restricted pore connectivity, and contact angle variations.

The capillary relation described above can be applied to pore structure models to estimate a grain-scale at which hysteresis in $S(\psi)$ vanishes. In a simple representation, a porous medium can be idealized as having two pore-sizes [Haines, 1930]. Pore bodies are interconnected to each other through narrower pore throats of radius R_t. These pore radii clearly scale in direct proportion to the medium's characteristic grain-size, denoted by λ. When λ and R_t are so large that capillary rise cannot even exceed a significant fraction (f) of λ, the "Haines jump" no longer occurs and hysteresis vanishes. In random packing of monodisperse spherical grains, local arrangements will typically be constrained between tetrahedral close-packing and cubic open packing. We will constrain f to be between 0.817 and 1, since these values represent the vertical spacing (in units of λ) separating pore throats in tetrahedral close-packing and cubic open packing of grains, respectively. Thus, we now need to identify the values of λ above which capillary rise does not reach 0.817λ and λ, and this depends on pore-size distributions. In order to apply (1), it will be useful to express R as a fraction (j) of λ. For the close-pack case, the pore throat radius controlling drainage can be assigned a value approximately equal to that of a circle bounded by 3 nearest-neighbor grains in tetrahedral arrangement. Thus, $R_t(close) \approx 0.0774\lambda$. Although one-third of the pores in close packs are rhomboidal [Haines, 1927], and larger than those bounded by tetrahedral grain packs, drainage of these larger pores is still controlled by $R_t(close)$ because of being surrounded by smaller pore throats of tetrahedral packs. For the open pack case, the pore throat can be approximated by a circle bounded by 4 coplanar, nearest-

neighbor grains such that $R_t(open) \approx 0.207\lambda$. Thus, the capillary rise height associated with drainage of this monodisperse system is

$$h_i \approx \frac{2\sigma}{\rho g j_i \lambda} \tag{2}$$

with $j_1 = 0.207$ (open-pack) and $j_2 = 0.0774$ (close-pack). By setting $h_i = f_i\lambda$, with $f_1 = 1$ (open-pack) and $f_2 = 0.817$ (close-pack), we obtain the estimated bounds for elimination of capillary hysteresis. Thus, the critical grain-size separating hysteretic and nonhysteretic systems is

$$\lambda_{c,i} \approx \sqrt{\frac{2\sigma}{f_i j_i \rho g}} \tag{3}$$

For $\sigma = 72$ mN m^{-1}, $\rho = 998$ kg m^{-3}, and $g = 9.81$ m s^{-2}, λ_c is estimated to be 8.4 mm and 15 mm for open- and close-packed systems of spherical grains, respectively. Since nominally monodisperse, rounded grains tend towards intermediate packing, their predicted λ_c is expected to occur between the above values. Narrower restrictions on λ_c can be obtained based on scaling of moisture characteristics of real granular media, as described next.

2.2. Haines-Miller-Miller scaling prediction

Another approach to identifying λ_c can be developed from the unsaturated hydraulic scaling methodology of Miller and Miller [1955a, 1956] and the conceptual model of Haines [1930]. The scaled matric potential, Ψ, is the product of matric potential times the characteristic grain-size, divided by the fluid-fluid surface tension. Thus, Ψ is related to the matric potential ψ and matric head h_m through

$$\Psi = \frac{\lambda \psi}{\sigma} \tag{4a}$$

and

$$\Psi = \lambda \frac{\rho g}{\sigma} h_m \tag{4b}$$

respectively. In Miller-Miller similar systems, drainage curves obtained on media of differing grain-sizes all fall on a single scaled desaturation curve, $S(\Psi)$. Likewise, their wetting curves collapse onto a single scaled wetting curve, $S(\Psi_w)$. Unscaled and scaled moisture characteristics for hypothetical Miller-Miller similar systems are illustrated in Figures 1a and 1b, respectively. With knowledge of the universal $S(\Psi)$ and $S(\Psi_w)$ relations, moisture retention relations in any other media that are approximately geometrically similar can be predicted. As noted by Miller and Miller [1955a], the early analyses of Haines [1927, 1930] reflected an appreciation for scaling through his choice of $2\sigma/\lambda$ as the unit of measure for the pressure variable. The validity of Miller-Miller scaling has been demonstrated on well-sorted sands over λ ranging from 0.05 to 1.1 mm by Miller and Miller [1955b], Klute and Wilkinson [1958], and Schroth et al. [1996]. The question mark placed alongside the hypothetical relation for $\lambda = 10$ mm in Figure 1 emphasizes the fact that the nature of moisture characteristics of very coarse media still require examination.

The fact that hysteresis is preserved in scaled saturation curves can now be used to predict the value of λ above which hysteresis vanishes. Two parameters useful for determining whether or not Miller-Miller similitude describes moisture characteristic curves of approximately monodisperse media are the drainage midpoint and wetting midpoint values of the scaled matric

potential, Ψ_{dm} and Ψ_{wm}, respectively. We define these values as the scaled potentials associated with 50% effective saturation, when the effectively fully desaturated state is assigned to Ψ = -35. This reference Ψ of -35 is somewhat arbitrary, but is associated with very small moisture capacities (very small $dS/d\Psi$), and "residual" saturations. Thus Ψ_{dm} and Ψ_{wm} are the scaled matric potentials associated with 50% effective saturation. These values are indicated by the triangles on the Figure 1 curves. Values of scaled drainage and wetting midpoint potentials from various studies are listed in Table 1. These data show that, for porous media composed of nearly monodisperse grains, scaled midpoint energies occur at fairly unique values of about –12 ±2 and –8 ±1 for draining and wetting, respectively. These values of Ψ_{dm} and Ψ_{wm} combined with (1) can be used to define effective pore-sizes associated with drainage and wetting. This approach leads to pore radii of about $\lambda/6$ and $\lambda/4$, for drainage and wetting, respectively. The drainage radius of $\lambda/6$ is equivalent to a j value of 0.167. This value of j is, as expected, between the previously calculated limiting values of $j_1 = 0.207$ (open-pack) and $j_2 = 0.0774$ (close-pack). We now approximate the porous medium as a bundle of capillaries having periodic variations in radii, R, bounded by the two limits, $\lambda/6$ and $\lambda/4$. Approximating the variation of R as having cosine dependence with respect to elevation and associating $f\lambda$ with the period of variation, the vertical profile for R is

$$R(z) = \frac{\lambda}{24}\left[5 + \cos\left(\frac{2\pi z}{f\lambda} + \delta\right)\right] \tag{5}$$

where z is elevation, and δ is an arbitrary phase lag. Periodicity is assumed to be between 0.817λ and λ, as previously described, i.e. $0.817 < f < 1$. Several $R(z)$ profiles are illustrated in Figure 2a, for $f = 1$. Potential equilibrium capillary head profiles, $H_m(z)$ are then obtained by combining (1) and (5),

$$-H_m(z) = \frac{48\sigma}{\rho g \lambda\left[5 + \cos\left(\frac{2\pi z}{f\lambda} + \delta\right)\right]} \tag{6}$$

Thus, $H_m(z)$ represents the matric head at any given position *if* the meniscus was located at that elevation. Example $H_m(z)$ profiles are shown in Figure 2b (again with f = 1), along with the hydrostatic equilibrium $h_m(z)$ profile for the case of a water table at z = 0. Our comparison between $h_m(z)$ and $H_m(z)$ profiles follows Haines [1930], in which a case similar to that for $\lambda = 4$ mm was illustrated. Referring to the example with λ = 4 mm in Figure 2b, Haines reasoned that drainage equilibrium coincides with point A, wetting equilibrium coincides with point B, and that point C is metastable and will equilibrate by the meniscus moving up to point D. The set of $H_m(z)$ profiles in Figure 2b illustrate several other predictions. From (6), it follows that the elevations associated with points of intersection between $h_m(z)$ and $H_m(z)$ profiles are the z_i roots to

$$\frac{48\sigma}{\rho g \lambda^2} - \left[5 + \cos\left(\frac{2\pi z_i}{f\lambda} + \delta\right)\right]\frac{z_i}{\lambda} = 0 \tag{7}$$

In this representation, hysteresis is possible when (7) has multiple roots, as just described for the case of λ = 4 mm. The multiplicity of intermediate potential equilibrium values reachable via reversing a wetting or draining process is further evident in the λ = 2 mm profile. As in the λ = 4 mm case, lower limits of metastable conditions are indicated in the small open circles, and their corresponding equilibrium points are the nearest overlying filled circles. The λ = 9 mm case

shows a condition where a short segment of its $H_m(z)$ profile is approximately overlapping with the $h_m(z)$ profile. The short vertical distance of about 2 mm (7 to 9 mm elevation) associated with this segment indicates that separation between draining and wetting curves will be very slight for $\lambda = 9$ mm. It should be noted that this overlap example for $\lambda = 9$ mm was obtained by setting $\delta = 2.32$, and that the intersection was more commonly only at a single elevation that varied slightly with δ. For $\lambda > 9.8$ mm, (7) contains only a single root (per given δ) when $f = 1$, and the $H_m(z)$ and $h_m(z)$ only intersected at a single, δ-dependent point, as illustrated for the $\lambda = 20$ mm case. By this approach, the elimination of capillary hysteresis is predicted to occur at $\lambda_c = 9.8$ mm, assuming cubic-pack periodicity ($f = 1$). Using the same procedure, but assuming tetrahedral close-packing ($f = 0.817$) leads to removal of hysteresis at $\lambda_c = 10.9$ mm. These last two calculations constrain values for λ_c in a randomly packed granular medium having a value of f between 0.817 and 1. Thus, our best estimate for the critical grain-size in monodisperse media with spherical grains is $\lambda_c = 10.4 \pm 0.5$ mm.

2.3. Combined influences of grain-size, surface tension and gravity

A broader perspective on this problem includes, in addition to grain-size, the influences of surface tension, fluid densities, and acceleration. These factors determine configurations of meniscii through determining body and surface forces, and their relative intensities can be expressed as dimensionless ratios. By analogy to the familiar Bond number (*Bo*),

$$Bo = \frac{\Delta\rho g R^2}{\sigma} \tag{8}$$

we define the Haines number as

$$Ha = \frac{\Delta\rho a \lambda^2}{\sigma} \tag{9}$$

where $\Delta\rho$ denotes the density difference between immiscible fluids (e.g., water and air) and a is the acceleration (usually that of ordinary gravity, g). The advantage of using *Ha* rather than *Bo* comes from referencing grain-size, a directly measured material property, rather than a calculated pore radius or interfacial radius of curvature. Recall that $\lambda_c = 10.4 \pm 0.5$ mm was associated with the predicted disappearance of hysteresis under standard conditions of water-air systems on the earth's surface ($a = g = 9.81$ m s^{-2}, $\Delta\rho = 997$ kg m^{-3}, and $\sigma = 0.072$ N m^{-1}). Using these values in (9) indicates that $Ha = 14.7 \pm 1.4$ is the general boundary separating hysteretic and nonhysteretic moisture characteristic relations. For brevity, this predicted critical value will be referred to as $Ha = 15$. The equivalent boundary in terms of the radius of curvature for drainage is obtained by recalling that $R_d \approx \tilde{\lambda}6$, which upon substitution into (9) yields a critical $Bo \approx 0.5$. Thus, our perception that hysteresis is a basic feature of unsaturated porous media is a consequence of the magnitudes of each term on the right hand side of (9), which ordinarily combine to keep $Ha < 15$. The dependence of *Ha* on grain-size is plotted for the usual values of $\Delta\rho$, $a = g$, and σ as the "standard case" in Figure 3. Additional curves for cases with lower surface tension ($\sigma = 24$ mN m^{-1}), much higher body force (samples in a centrifuge at $a = 1{,}000g$), and oil-water systems ($\Delta\rho = 50$ kg m^{-3}, and $\sigma = 20$ mN m^{-1}) are also shown in Figure 3. The above analysis indicates that measurements involving lower surface tension will exhibit loss of hysteresis at smaller grain-sizes. A test of this prediction is included in the experimental section of this study. With respect to higher body forces, it should be noted that centrifuge methods are typically not used for quantifying the high (closer to zero) matric potential region of $S(\psi)$

relations. Nevertheless, this analysis indicates that if coarse sands were equilibrated under high centrifugal forces, they will not exhibit hysteretic moisture characteristics, and therefore such measurements could not be used to predict drainage and wetting curves under ordinary gravity. Conversely, unsaturated equilibrium in lower gravitational fields will support hysteresis at $\lambda >$ 10.4 mm (for $\Delta\rho = 997$ kg m^{-3}, and $\sigma = 72$ mN m^{-1}). The oil-water example in Figure 3 serves to illustrate that hysteresis in hydrophilic media will also be retained up to larger grain-sizes since effects of much smaller fluid density differences will typically outweigh effects of lower surface tension. In the limit of microgravity conditions (e.g. Jones and Or, 1999), we predict that hysteresis will be preserved to extremely coarse scales. In very coarse gravels under microgravity, capillary water films (Tokunaga and Wan, 1997, 2001) are expected to strongly influence unsaturated flow.

As an aside, we note that the condition of microscopic geometric similitude is lost before the predicted limit for saturation hysteresis is reached. The similitude condition on which Miller-Miller scaling is based requires that variations in interfacial curvature be insignificant at the pore level, at any given ψ. A simple illustration of this condition involves a trapped, approximately spherical, air bubble of radius R contained in a pore body. The hydrostatic pressure difference between the bottom and top points on the bubble is

$$\Delta P_{j,i} \approx 2\rho g R_j \approx \frac{2\sigma}{R_j} - \frac{2\sigma}{R_i} \tag{10}$$

where R_i and R_j are now take as the radii of curvature for the lower and upper hemispheres, respectively. Rearranging (10) gives

$$\frac{\rho g R_j^2}{\sigma} = Bo \approx 1 - \frac{R_j}{R_i} \tag{11}$$

The above expression shows that pore-scale variations in interfacial curvature are insignificant only when R_i and R_j are nearly identical, and $Bo \approx 0$. Recall that $Ha = 15$ was associated with $Bo \approx 0.5$, indicating that geometric similitude is lost before the predicted disappearance of hysteresis.

3. Materials and Methods

The simplest test of the above analyses involves measuring draining and wetting moisture characteristic relations in a series of sand and gravel columns, and seeing if hysteresis vanishes above the predicted value of λ. To our knowledge, no such data for gravels were previously available. A complication encountered in measurements on unsaturated coarse granular media is that moisture profiles within equilibrium columns are uniform only in the limit of low saturation. At higher saturations, the equilibrium saturation profile is stratified because of the relatively strong influence of gravity. Values of saturation are higher within lower sections of sample columns, reflecting the equilibrium balance between matric and gravitational potentials. Various approaches to accounting for stratification of the moisture profile have been developed [Liu and Dane, 1995; Schroth et al., 1996; Jalbert and Dane, 2001; Tokunaga et al., 2002]. The method developed by Tokunaga et al. [2002] is used in the present work, with small incremental changes applied in the reservoir boundary potential (typically 5 to 10 mm changes in head). A modification of our previous apparatus was developed to eliminate the need for periodic adjustments of reservoir water levels during individual equilibration steps. This modification was used with a few of the measurements on gravels and is described next.

A large Tempe Pressure Cell (Soilmoisture Equipment Corp., Santa Barbara, CA) was modified to determine the moisture characteristics of the sands and most of the gravels used in this study (Figure 4). The brass sample chamber was replaced with an 82.6 mm I.D., 3.2 mm wall thickness, 30 to 70 mm high acrylic tube. A 50 kPa air-entry, high flow, ceramic plate (Soilmoisture Equipment Corp.) was used to control the potential along the lower boundary of the sand samples. For the gravel samples, a 4.4 kPa air-entry glass frit (Porous C plate, Ace Glass, Vineland, NJ) was used since only low magnitude suctions needed to be applied. The outlet on the bottom end cap was drilled and tapped (1/8" NPT) in order to securely attach a 3-way valve. The 3-way valve allowed for switching the flow path from a horizontal volume-indicating reservoir (burette) to either the sample cell or to a second 3-way valve that allowed draining or filling. There were no direct paths between the cell and the reservoirs, alleviating accidental sample draining or filling. The acrylic burette had an I.D. of 3.1 mm, and measured advancing and receding capillary rise values of 2.0 ±1 and 4.5 ±1 mm, respectively (surfactant-free water at room temperature). The potential was regulated by setting the horizontal burette at specific elevations relative to the sample. Systematic small vertical offsets of 2.0 and 4.5 mm were applied to burette elevations in an attempt to compensate for capillary influences. The burette was calibrated to a resolution of 0.01 mL ($\approx 2 \times 10^{-4}$ of a typical sample pore volume), and was clamped to vertical rulers indicating elevation relative to a reference plane in the sample.

The sand or gravel was packed into the cell to a density of 1.54 ±0.06 Mg m^{-3}. Packing heights ranged from 30 to 60 mm. Samples were saturated by filling the cell with degassed water from the bottom, up to a height of 1 to 2 mm above the pack, and then drained overnight to remove excess water from the top of the pack. In coarser ($\geq$ 7 mm) gravels, the starting water level was set at the nominal mid-plane of the uppermost layer of grains in order to minimize influences of higher porosity at this boundary. At the start of an experiment, the nearly empty burette would be moved down to a new position while maintained in its horizontal orientation, and outflow volumes would be monitored. When the outflow rate was less than 0.01 mL h^{-1}, the burette was drained and lowered to the next step. This procedure was repeated until a residual saturation condition was approached. At this point, the burette would be filled with water for rewetting the sample, and have its elevation raised through a series of steps to progressively resaturate the gravel or sand pack. Like in the draining steps, the volume of inflow would be monitored and that particular step would conclude when the inflow was less then 0.01 mL hr^{-1}. Equilibration times between step changes ranged from 1 hour to 14 days. Equilibration head change increments were as small as 5 mm (gravels and most sands), and as large as 315 mm (finer sand). When the burette height reached the top of the pack, the experiment was completed.

A variation on the method just described was applied for measurements on the largest grain-size gravels (13-16 mm sieve interval). Because of its very large grain-size, packing of this gravel fraction into the Tempe cells would have resulted in variable pore-size and porosity profiles. One possible remedy to this problem would involve running multiple moisture characteristics, each time repacking with the same material. Instead, a column with a larger inside diameter (216 mm) was used. Preliminary tests on these largest gravels showed that capillary rise was less than their characteristic grain-size, and that they were effectively at residual saturation (S_{res}) at elevations greater than about 3 mm above the water table, regardless of wetting history. These observations motivated an alternative procedure (applicable only when capillary rise $< \lambda$), involving raising and lowering the water table within the gravel column without use of a porous plate, and analyzing results in terms of a step-function moisture

characteristic model. Assuming that capillary rise in very coarse gravels still scales approximately as $\sigma\lambda^{-1}$, we have $h \approx b\sigma\lambda^{-1}$. The surface tension is kept as an independent parameter here because its influence is tested in one experiment, while density and gravity terms are lumped into the parameter b since they are not varied. The empirical parameter $b \approx 6 \times 10^{-4}$ N^{-1} m^3, based on the 3 mm rise observed in the nominally 14 mm gravel, with $\sigma = 71$ mN m^{-1}. A porous medium that conforms exactly to this description can be described through

$$S = S_{res}, \quad h_m < \frac{-b\sigma}{\lambda} \tag{12a}$$

$$S = 1, \quad h_m > \frac{-b\sigma}{\lambda} \tag{12b}$$

The volume-averaged saturation, $\overline{S}$, within a column of height L that conforms to such a step function moisture characteristic is then

$$\overline{S} = 1, \qquad h_{m,ref} > L - \left(z_{ref} + \frac{b\sigma}{\lambda} \right) \tag{13a}$$

$$\overline{S} = S_{res} + (1 - S_{res}) \frac{h_{m,ref} + z_{ref} + \frac{b\sigma}{\lambda}}{L}, \qquad -\left(z_{ref} + \frac{b\sigma}{\lambda} \right) \le h_{m,ref} \le L - \left(z_{ref} + \frac{b\sigma}{\lambda} \right) \tag{13b}$$

and

$$\overline{S} = S_{res}, \qquad h_{m,ref} < -\left(z_{ref} + \frac{b\sigma}{\lambda} \right) \tag{13c}$$

where $h_{m,ref}$ refers to the matric (pressure) head at the arbitrary reference elevation in the sample, and z_{ref} is the elevation of this reference plain relative to the base of the sample. Within the range where water is draining from the gravel, the column-averaged moisture capacity is the derivative of (13b)

$$\frac{d\overline{S}}{dh_{m,ref}} = \frac{(1 - S_{res})}{L} \tag{14}$$

Systems that can be described by (13) and (14) support applicability of (12a,b). More importantly, when average saturations obtained in drainage and wetting processes both conform to (13) and (14), nonhysteretic $S(\psi)$ is demonstrated to within experimental uncertainty.

Most of the sands and gravels were obtained from the Hanford Formation, as described previously [Tokunaga et al., 2002]. Sands and gravels were sieved into 0.21-0.25, 0.42-0.50, 1.0-1.2, 2.2-2.4, 2.4-3.4, 4.8-5.3, 6.3-8.0, 8.0-9.5, and 9.5-11.2 mm size fractions for testing of approximately monodisperse media. These samples will be referred to as 0.2, 0.5, and 1 mm sands, and 2, 3, 5, 7, 9, and 10 mm gravels, respectively. Because of insufficient quantities of greater than 10 mm gravels in our supply from Hanford, tests of the largest size fraction were done on the 13-16 mm sieved fraction of commercially purchased river gravel. A 6.3-8.0 mm sieved fraction of river gravel was also used. These samples will be referred to as 14 and 7 mm river gravels. The overall shapes of the sands and gravels were similar, having sphericities of about 0.7 and roundness of about 0.6 [Krumbein and Sloss, 1963]. Data on drainage curves for the 2, 5, and 9 mm gravels have been presented previously [Tokunaga et al., 2002].

The 7 mm Hanford gravel was tested with distilled water and with a surfactant solution in order to test the influence of surface tension on capillary hysteresis. All surface tension

measurements were obtained with a Wilhelmy plate tensiometer (K10ST, Kruss USA, Charlotte, NC), at room temperature. Solutions of the surfactant, sodium dodecylbenzenesulfonate (SDBS), were prepared at a concentration of 10 mM. This solution had an initial σ = 31.5 ±0.2 mN m^{-1} before exposure to the gravel, and a final σ = 26.5 ±0.2 mN m^{-1} after equilibration with the gravel. Surface tension measurements of distilled water equilibrated for 2 days with Hanford gravel yielded σ = 70.8 ±0.6 mN m^{-1}. With these values of σ, *Ha* ≈ 7 and 18, for the 7 mm gravel interacting with water and 10 mM SDBS, respectively. Since the proposed critical *Ha* = 15 is between these values, hysteresis is predicted to exist with water, but not with the surfactant solution. The gravel was saturated with the SDBS solution through purging about 5 pore volumes of the solution and overnight hydrostatic ponding prior to initiating moisture retention measurements. The stable, low σ of the SDBS solution, and its practically perfect wetting of acrylic plastic allowed experiments to be done without applying different head corrections to the burette for drainage and filling steps. In addition to the 7 mm Hanford gravel, 7 mm river gravel was also used in the surface tension tests.

4. Results and Discussion

Both drainage and wetting curves were obtained on all of the samples except for the 0.5 mm sand, which had an air leak upon completion of its drainage curve. For brevity, individual plots of $S(\psi)$ will be presented for selected grain-sizes (0.2, 2, 5, 9, 10, and 14 mm), and midpoint energies from all samples will be presented later in a single figure. The individual unscaled drainage and wetting curves are shown in Figures 5 through 10. Column-averaged *S* data are shown as points, while gravity-corrected $S(h_m)$ are presented as curves. Comparisons of these figures show that gravity-corrections of drainage and wetting curves become progressively more important for larger grain-sizes. For grain-sizes less than 2 mm (i.e., the 0.2, 0.5, and 1 mm sands), no measurable differences were obtained between column-averaged *S* and gravity-corrected *S* values. It is apparent the "residual" saturations are fairly high in all of the Hanford sands and gravels. Most of the water associated with high residual saturation in these sands and gravels resides in nanometer to submicrometer intragranular pores, and is relatively immobile [Tokunaga et al., 2003]. Comparisons among the moisture characteristics (Figures 5 through 10) also show that drainage and wetting curve hysteresis becomes less distinct in coarser textured media. It should be noted that all of the measurements share similar energy uncertainties (from ±1 to ±2 mm matric head), which is insignificant in fine-grained media but is progressively more influential in coarser gravels. At λ = 9 and 10 mm, drainage and wetting curves are barely distinguishable, and at λ = 14 mm they are identical. Note that application of the gravity correction procedure on the 10 mm gravel data yields noisy results at intermediate ψ, probably because of the relatively small number of grains contained in the Tempe cell and consequent variation in porosity. Nevertheless, a narrow hysteresis loop is still detectable at λ = 10 mm, and supported by good reproducibility of the duplicate runs (Figure 10). Thus, the upper λ limit for hysteretic $S(\psi)$ under standard conditions occurs between 10 and 14 mm. Because of the quadratic dependence of *Ha* on λ, these limits only constrain the critical Haines number between 14 and 27.

Another perspective on the approach towards removal of hysteresis with increased λ can be obtained by examining scaled midpoint potentials. Scaled matric potential values at midpoints for drainage and wetting were obtained from the gravity-corrected results of all the samples, and plotted with respect to grain-size in Figure 11. Also shown in this figure are values of scaled midpoint matric potentials from the literature (listed in Table 1). Over most of the tested range of

λ, our scaled drainage and wetting midpoint potentials are within the range previously reported for sands. At large λ, increases in scaled potentials at midpoints are evident from the drainage curves, while wetting curves are less variable. The increases in scaled midpoint potentials reflect progressive deviations from Miller-Miller similitude. At the largest measured grain-size (λ = 14 mm), scaled midpoint potentials for drainage and wetting are identical, but nonzero. The finite magnitude of midpoint matric potentials in this limit results from small capillary rise that scales approximately inversely with λ. Combining (4b) and (12a,b) shows that Ψ_{dm} and $\Psi_{wm} \approx -6$ in systems lacking hysteresis, regardless of grain-size.

The measurements on the 7 mm Hanford gravel with water (*Ha* = 7) and with SDBS (*Ha* = 18) are shown in Figure 12. With water (Figure 12a), these gravels retained hysteretic moisture characteristics. Hysteresis was removed upon addition of SDBS (Figure 12b), in accordance with the predicted surface tension effect. Practically identical results were obtained for the 7 mm river gravel (data not shown). The step-function approximation for nonhysteretic moisture retention, (12) and (13), was applied to the SDBS system and compares fairly well with column-averaged saturations and with corrected retention curves (Figure 12b). This surface tension experiment on 7 mm gravel restricts the upper limit of hysteretic $S(\psi)$ to the range of $7 < Ha < 18$. Combining this result with those obtained by varying λ leads to the general, experimentally supported limit for hysteretic $S(\psi)$ occurring within the range of $14 < Ha < 18$. Recall that our predicted critical condition was $Ha = 14.7 \pm 1.4$.

Although the magnitude of λ_c was not predicted by Miller and Miller [1956], they did anticipate the existence of a grain-size limit to capillary scaling. They noted that the discreteness of grain- and pore-size can not be simply treated in a continuum manner at very large λ. Furthermore, their analysis requires that the product of the microscopic length (λ) times the characteristic macroscopic length L (e.g., height of soil columns) be constant in similar systems (at constant σ). Thus, systems with larger λ must be macroscopically smaller (shorter) in order to preserve similar unsaturated hydraulic characteristics. In the limit of very large λ, the discrete granular nature of systems is incompatible with the macroscopic continuum treatment applied for smaller λ.

Unsaturated states in coarse granular systems have a distinct property when considered from the perspective of soil water thermodynamics [Sposito, 1981]. In contrast to hysteretic soil systems, all states on the moisture characteristic relation of very coarse media with $Ha > 16 \pm 2$ are truly equilibrium states, attainable through infinitesimal, reversible steps from any initial condition. It is only in this limit of very large λ and/or a that pre-Haines models assuming nonhysteretic moisture retention are correct.

5. Summary

This study on moisture characteristics sought to predict the grain-size above which capillary hysteresis vanishes. Based on pore geometries of close-pack and open-pack spheres, the critical grain-size was estimated to be between 8 and 15 mm. A more constrained grain-size range of 9.8 to 10.9 mm was obtained based on Miller-Miller scaling and the hysteresis model of Haines. In both approaches, removal of hysteresis is associated with the condition that capillary rise does not extend up even a single grain height. More generally, critical grain-sizes are expected to depend on magnitudes of surface tension (not necessarily ≈ 72 mN m^{-1}) and the body force (not necessarily that of water-air systems under the influence of gravity at the earth's surface). The general threshold for removal of capillary hysteresis in monodisperse granular media was predicted to depend on the Haines number.

Experimental tests were conducted through measuring moisture characteristics of sands and gravels over grain-sizes ranging from 0.2 to 14 mm. Measurements on gravels required corrections for gravity-stratified equilibrium S profiles. Scaled midpoint matric potentials increased with increased grain-size. Based on measurements, the critical λ above which capillary hysteresis vanishes occurs between 10 and 14 mm (under standard conditions). The predicted influence of surface tension was demonstrated through measurements on 7 mm gravel, without and with SDBS, which exhibited and did not exhibit hysteresis, respectively. The collective evidence obtained in this work indicates that $Ha = 16 \pm 2$ is the limit above which hysteresis vanishes. The lack of previous awareness of nonhysteretic moisture characteristics appears to result from the fact that the combinations of λ, σ, $\Delta\rho$, and a considered have usually been within the realm of $Ha < 16 \pm 2$.

Acknowledgments. This paper is gratefully dedicated to TKT's graduate advisor, Lawrence Waldron, who introduced students to classic works such as that of Haines, and inspired inquiries into the physics of soil processes. We thank Andrew Mei of LBNL for technical support, and John Zachara, Robert Lenhard, Steve Smith, and Bruce Bjornstad of PNNL for samples of Hanford formation sediment. Helpful internal review comments by Rohit Salve (LBNL) and additional very constructive suggestions by two anonymous reviewers are gratefully acknowledged. This work was carried out under U.S. Dept. of Energy (DOE) Contract No. DE-AC03-76SF00098, with funding provided by the DOE, Basic Energy Science, Geosciences Research Program, and the Environmental Management Science Program.

References

Buckingham, E., Studies on the movement of soil moisture, U.S. Dept. Agric., Bureau of Soils Bulletin No. 38, Government Printing Office, Washington, DC, 1907.

Dullien, F. A. L. Porous Media Fluid Transport and Pore Structure, 2nd Ed. Academic Press, San Diego, 1992.

Fisher, R. A., Further note on the capillary forces in an ideal soil, *J. Agric. Sci., 18*, 406-410, 1928.

Gregg, S. J., and K. S. W. Sing. Adsorption, Surface Area and Porosity, 2nd Ed. Academic Press, London, 1982.

Haines, W. B., Studies in the physical properties of soil, IV. A further contribution to the theory of capillary phenomena in soil, *J. Agric. Sci., 17*, 264-290, 1927.

Haines, W. B., Studies in the physical properties of soil, V. The hysteresis effect in capillary properties, and the modes of moisture distribution associated therewith, *J. Agric. Sci., 20*, 97-116, 1930.

Jalbert, M., and J. H. Dane, Correcting laboratory retention curves for hydrostatic fluid distributions, *Soil Sci. Soc. Am. J., 65*, 648-654, 2001.

Jones, S. B., and D. Or, Microgravity effects on water flow and distribution in unsaturated porous media: Analyses of flight experiments, *Water Resour. Res. 35*, 929-942, 1999.

Klute, A., and G. E. Wilkinson, Some tests of the similar media concept of capillary flow: 1. Reduced capillary conductivity and moisture characteristic data, *Soil Sci. Soc. Am. Proc., 22*, 278-281, 1958.

Krumbein, W. C., and L. L. Sloss. Stratigraphy and Sedimentation, 2nd Ed. W. H. Freeman and Co., NY, 1963.

Leverett, M. C., Capillary behavior in porous solids, *Trans. Am. Inst. Mining Metallurgical Eng.,*

142, 152-169, 1941.
Liu, H. H., and J. H. Dane, Improved computational procedure for retention relations of immiscible fluids using pressure cells. *Soil Sci. Soc. Am. J., 59*, 1520-1524, 1995.
Miller, E. E., and R. D. Miller, Theory of capillary flow: I. Practical implications, *Soil Sci. Soc. Am. Proc. 19*, 267-271, 1955a.
Miller, R. D., and E. E. Miller, Theory of capillary flow: II. Experimental information, *Soil Sci. Soc. Am. Proc. 19*, 271-275, 1955b.
Miller, E. E., and R. D. Miller, Physical theory for capillary flow phenomena, *J. Appl. Phys. 4*, 324-332, 1956.
Morishige, K., and N. Tateishi, Adsorption hysteresis in ink-bottle pore, *J. Chem. Phys. 119*, 2301-2306, 2003.
Ravikovitch, P. I., and A. V. Neimark, Density functional theory of adsorption in spherical cavities and pore size characterization of templated nanoporous silicas with cubic and three-dimensional hexagonal structures. *Langmuir 18*, 1550-1560, 2002.
Richards, L. A., The usefulness of capillary potential to soil moisture and plant investigators, *J. Agric. Res. 37*, 719-742, 1928.
Schroth, M. H., S. J. Ahearn, J. S. Selker, and J. D. Istok, Characterization of Miller-similar silica sands for laboratory hydrologic studies. *Soil Sci. Soc. Am. J., 60,* 1331-1339, 1996.
Sposito, G. *The Thermodynamics of Soil Solutions*, 223 pp., Oxford Univ. Press, New York, 1981.
Tokunaga, T. K., and J. Wan, Water film flow along fracture surfaces of porous rock, *Water Resour. Res*., 33, 1287-1295, 1997.
Tokunaga, T. K., and J. Wan, Approximate boundaries between different flow regimes in fractured rocks, *Water Resour. Res*., 37, 2103-2111, 2001.
Tokunaga, T. K., J. Wan, and K. R. Olson, Saturation-matric potential relations in gravel, *Water Resour. Res*., 38(10), 1214, doi:10.1029/2001WR001242, 2002.
Tokunaga, T. K., K. R. Olson, and J. Wan, Moisture characteristics of Hanford gravels: Bulk, grain-surface, and intragranular components, *Vadose Zone J., 2*, 322-329, 2003.
Topp, G. C. and E. E. Miller, Hysteretic moisture characteristics and hydraulic conductivities for glass beads, *Soil Sci. Soc. Am. Proc., 30*, 156-162, 1966.
Wan, J., and T. K. Tokunaga, Film straining of colloids in unsaturated porous media: Conceptual model and experimental testing, *Environ. Sci. Technol., 31*, 2413-2420, 1997.

material	grain-size, μm	porosity	Ψ_{dm}	Ψ_{wm}	source
glass spheres	380	0.37	13.7	8.7	Haines, 1930
sand	160	0.39	11.0	8.0	Leverett, 1940
sand	110	0.38	11.8	7.5	Klute and Wilkinson, 1958
sand	160	0.38	12.7	8.0	
sand	230	0.37	13.0	8.0	
glass beads	180	0.33	10.9	6.8	Topp and Miller, 1966
sand	360	0.35	10.9		Schroth et al, 1996
sand	530	0.35	10.8		
sand	710	0.35	10.0		
sand	1,110	0.35	10.6		
sand	180	0.35	13.5	8.9	Wan and Tokunaga, 1997
sand	450	0.34	11.5	8.1	

Table 1. Scaled matric potentials at drainage and wetting midpoints for glass beads and sands having narrow grain-size distributions (within ±20% of mid-range grain-size).

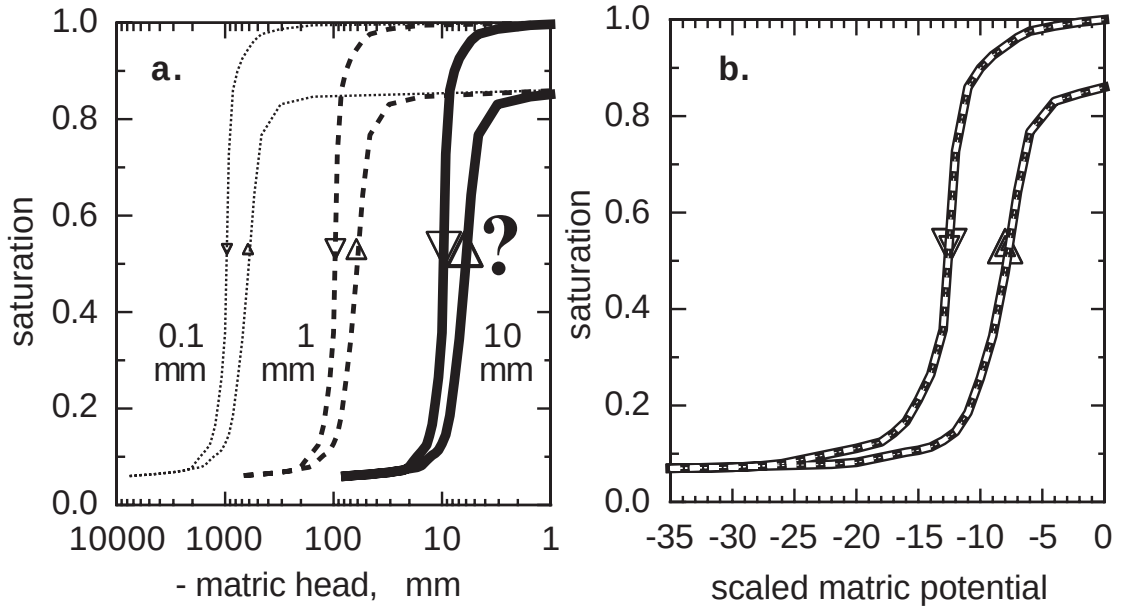

Figure 1. Hypothetical (a) unscaled and (b) Miller-Miller scaled moisture characteristic relations for porous media comprised of 0.1, 1, and 10 mm grains. A question mark is placed along the 10 mm grain-size curves to emphasize the fact that saturation-potential relations in very coarse granular media have not previously been determined. Midpoints on these drainage and wetting curves are indicated by triangles.

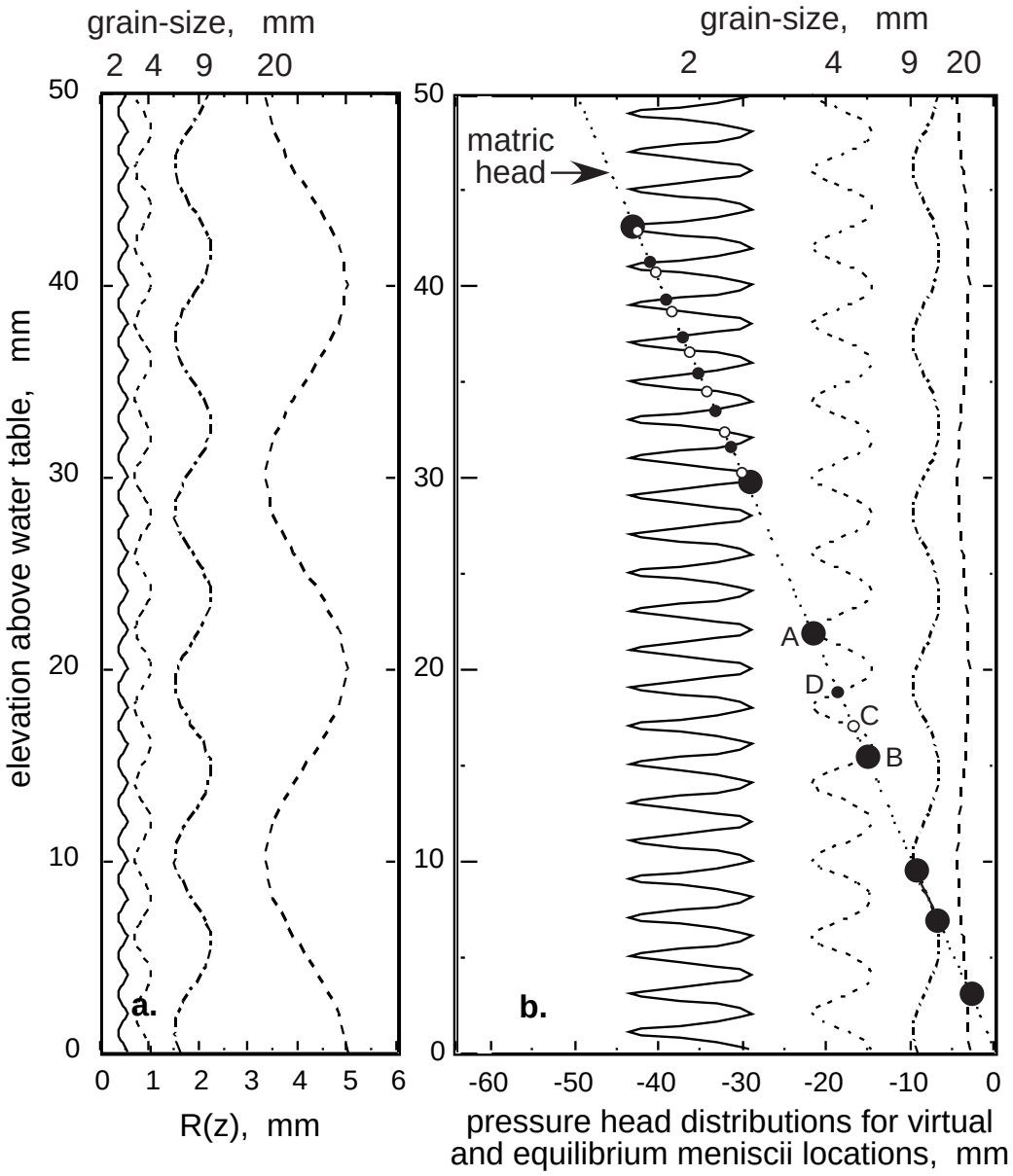

Figure 2. (a) Profiles of periodic pore-size variation with elevation for model systems having 2, 4, 9, and 20 mm grain-sizes. (b) Profiles of capillary pressure head, $H_m(z)$, associated with pore-sizes shown in panel a. The diagonal line represents the matric head profile at hydrostatic equilibrium, $h_m(z)$. Larger filled circles denote equilibrium meniscii elevations obtained for drainage (uppermost) and wetting (lowermost) for any given grain-size. Small open circles denote intermediate locations of minimum rise, while small filled circles indicate intermediate equilibrium meniscii elevations. See text for description of points A through D on the 4 mm grain-size profile.

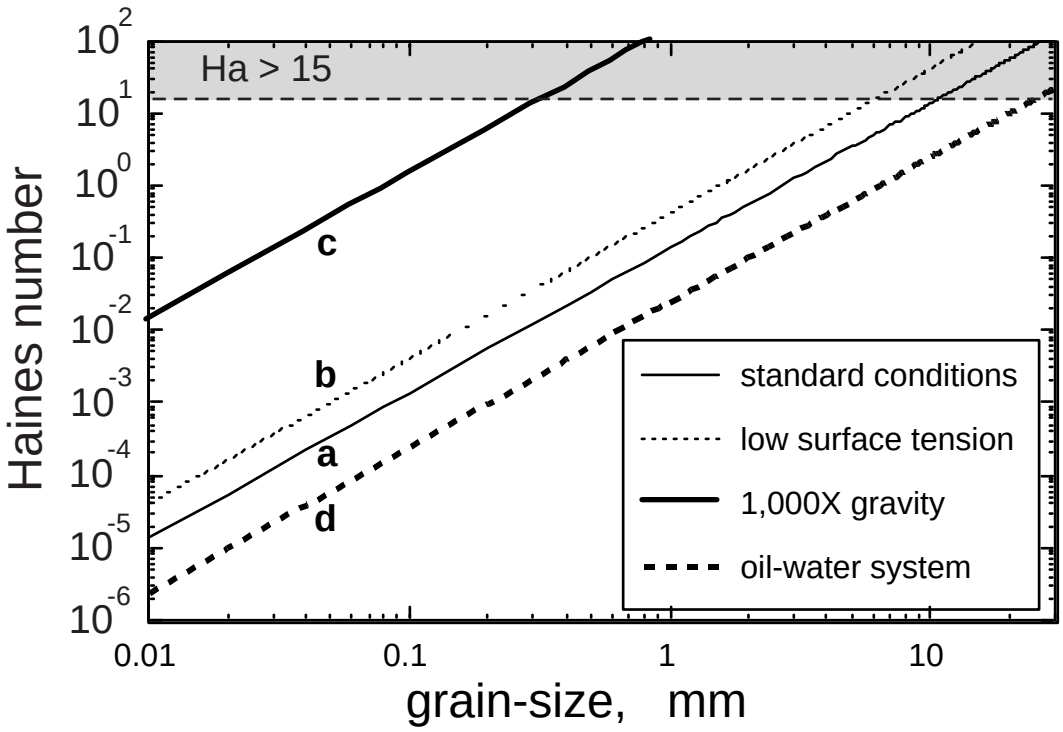

Figure 3. Grain-size dependence of the Haines number for (a) standard conditions (g = 9.81 m s^{-2}, $\Delta\rho$ = 997 kg m^{-3}, and σ = 0.072 N m^{-1}), (b) low surface tension (σ = 0.024 N m^{-1}, g = 9.81 m s^{-2}, and $\Delta\rho$ = 997 kg m^{-3}), (c) much higher body force (1,000X g, $\Delta\rho$ = 997 kg m^{-3}, and σ = 0.072 N m^{-1}), and (d) an oil-water system (g = 9.81 m s^{-2}, $\Delta\rho$ = 50 kg m^{-3}, and σ = 0.020 N m^{-1}). The horizontal line at *Ha* = 15 separates systems that do and that do not exhibit hysteresis.

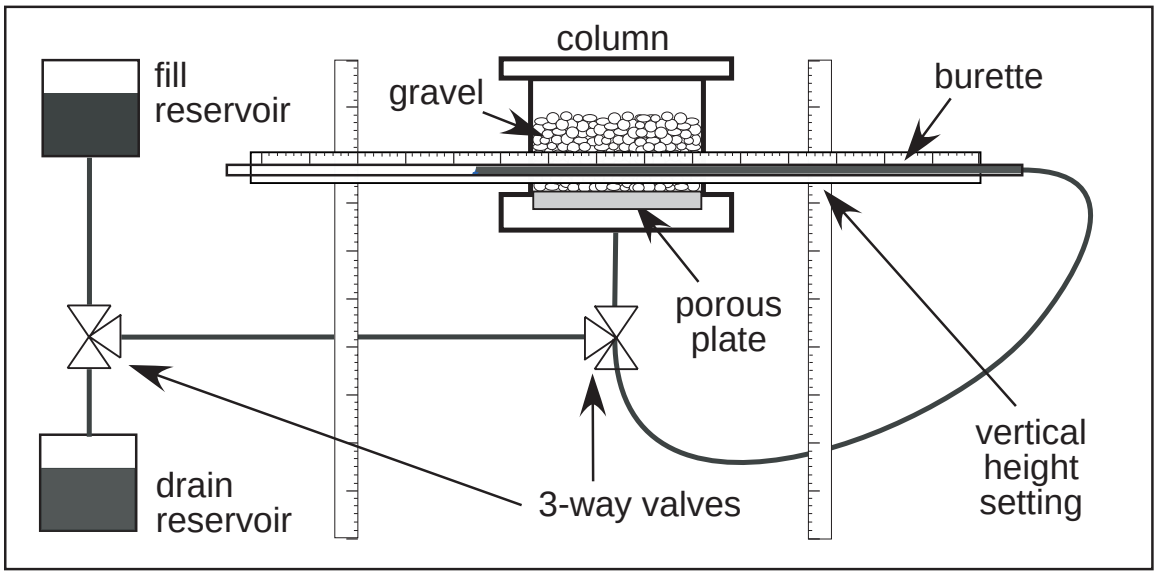

Figure 4. Apparatus for measuring moisture characteristics at near-zero matric potentials.

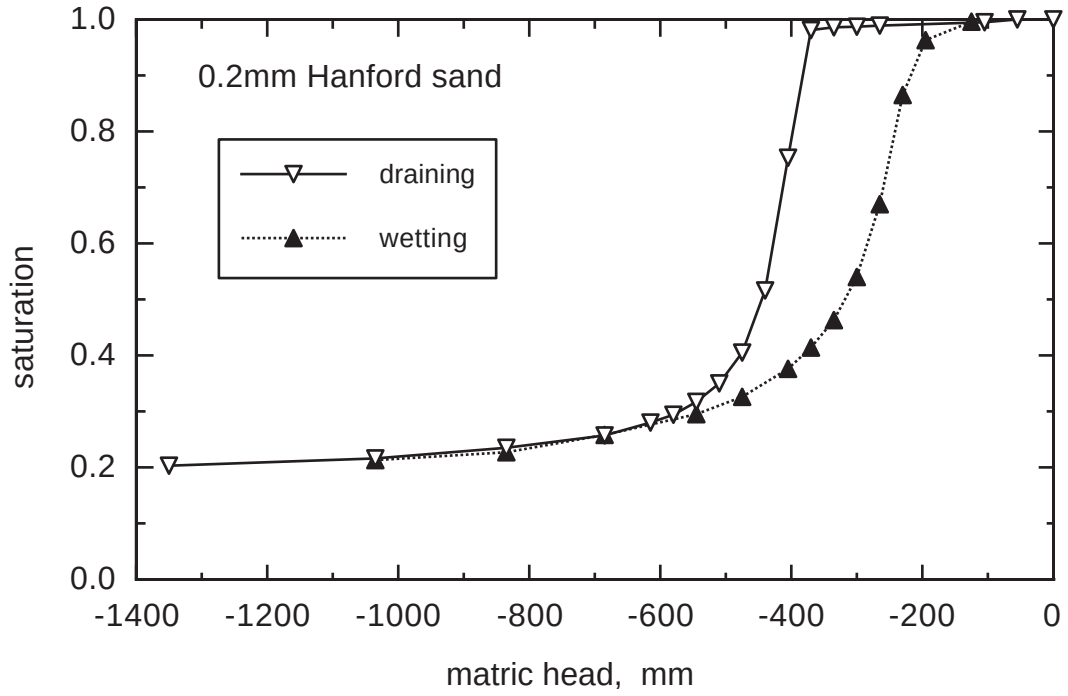

Figure 5. Moisture characteristic curves for 0.2 mm Hanford sand.

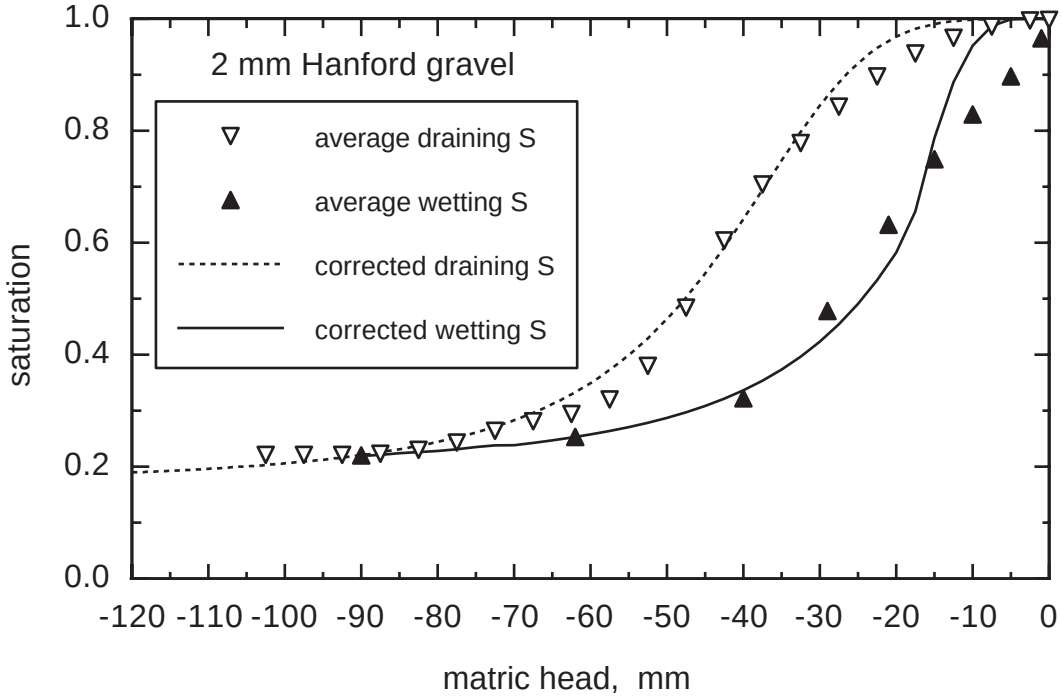

Figure 6. Moisture characteristic curves for 2 mm Hanford gravel.

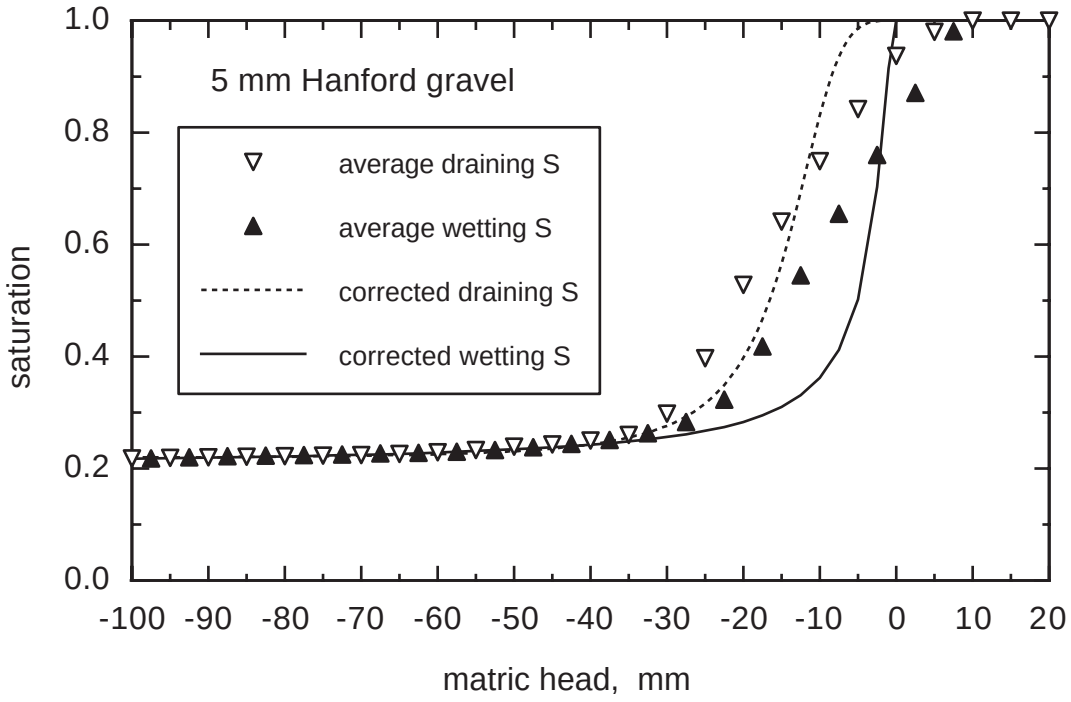

Figure 7. Moisture characteristic curves for 5 mm Hanford gravel.

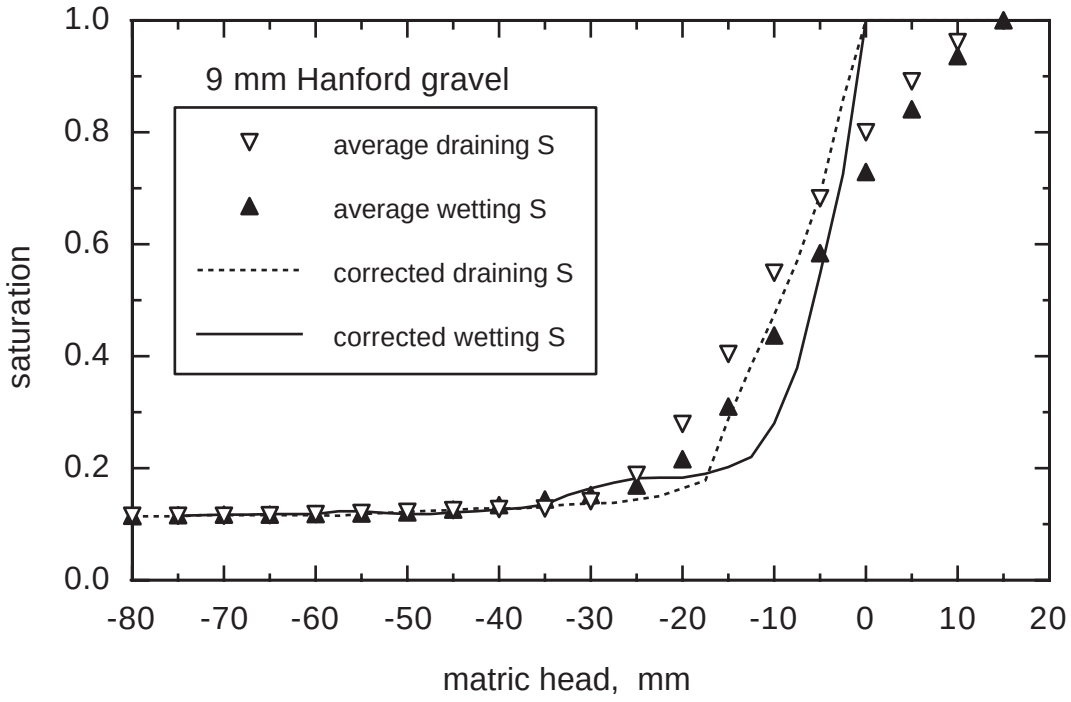

Figure 8. Moisture characteristic curves for 9 mm Hanford gravel.

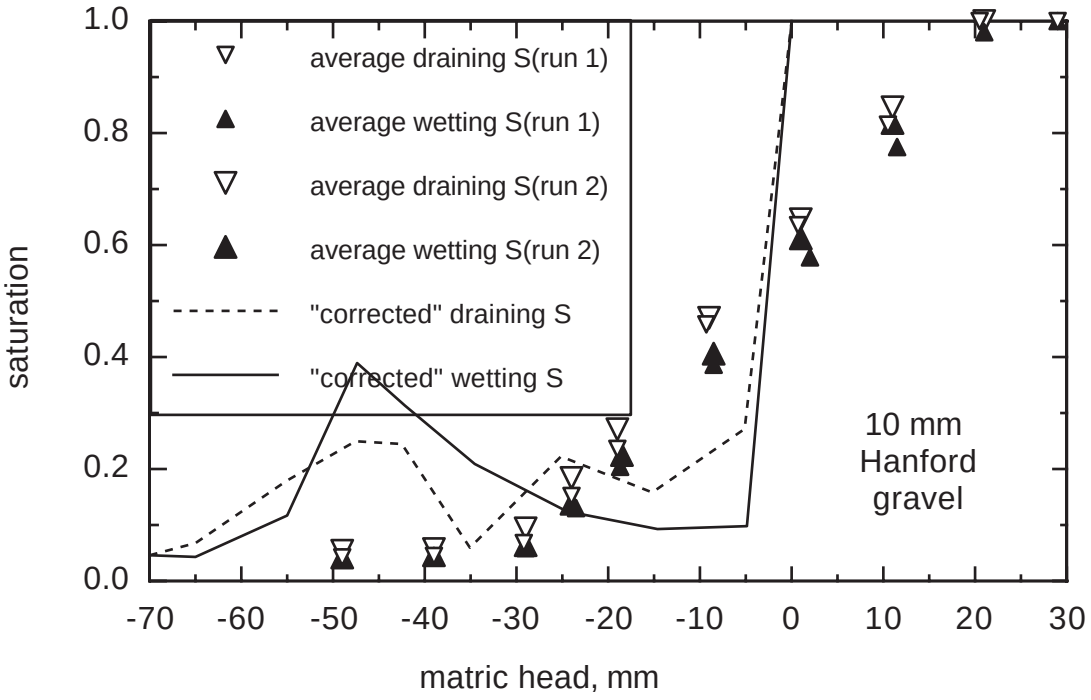

Figure 9. Moisture characteristic curves for 10 mm Hanford gravel.

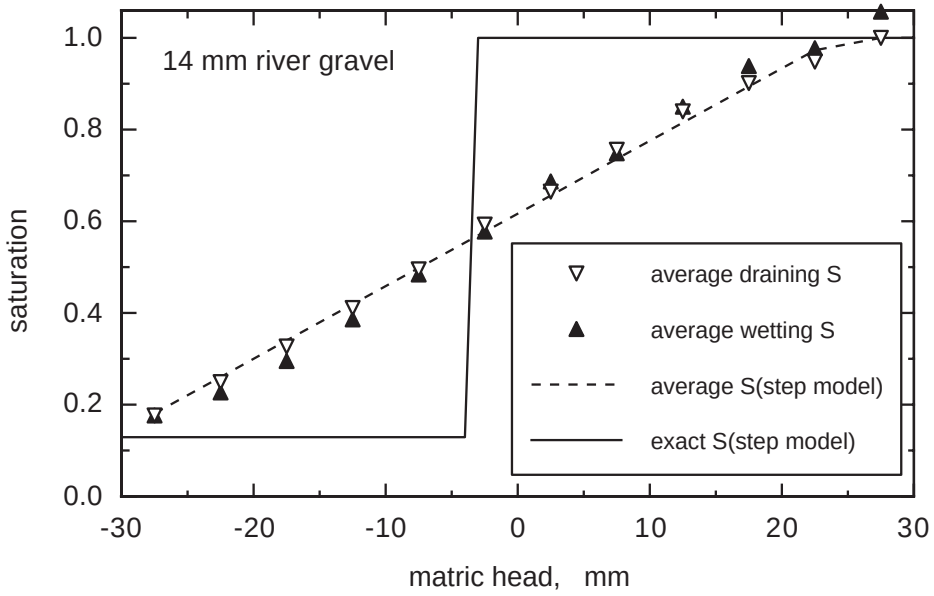

Figure 10. Moisture characteristic curves for 14 mm gravel.

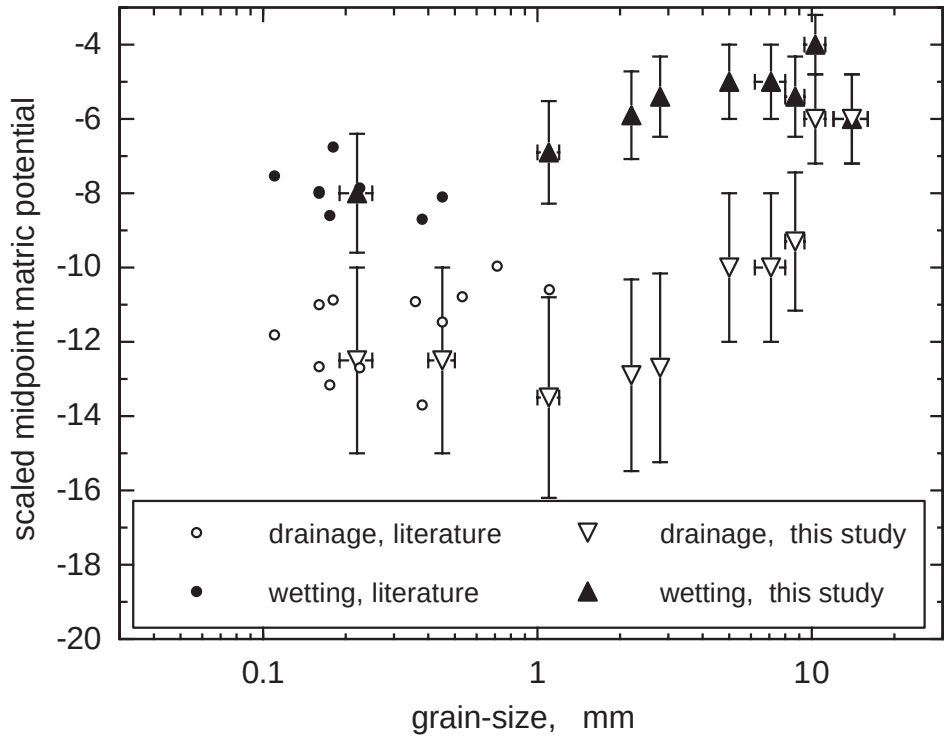

Figure 11. Dependence of scaled midpoint matric potentials on grain-size in monodisperse sands and gravels.

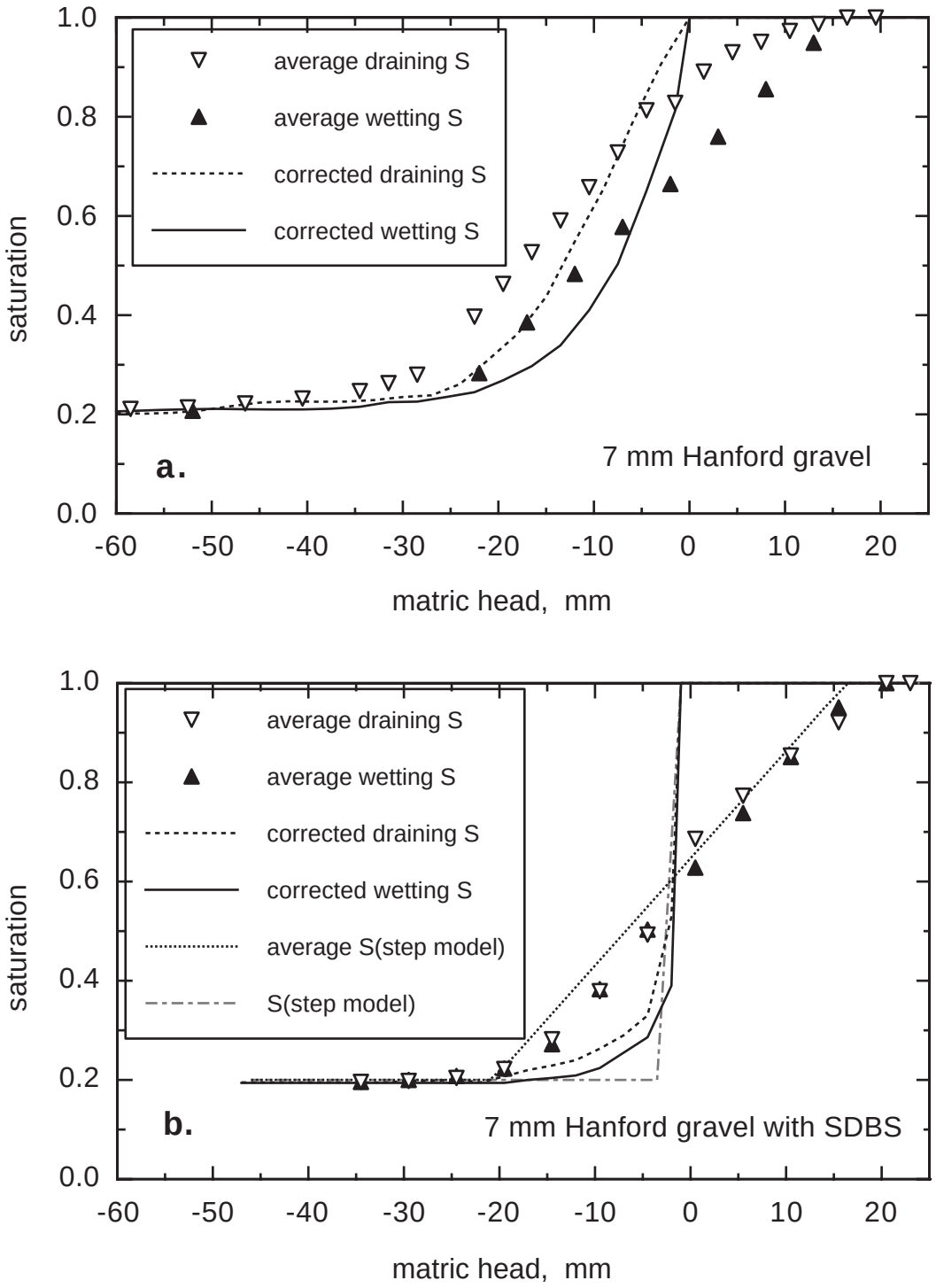

Figure 12. Moisture characteristic curves for 7 mm Hanford sand, (**a**) with water, and (**b**) with 10 mM SDBS solution.